


Sound absorption of petal shaped micro-channel porous materials

Cite as: Phys. Fluids **33**, 063606 (2021); <https://doi.org/10.1063/5.0053059>

Submitted: 04 April 2021 . Accepted: 30 May 2021 . Published Online: 15 June 2021

Wei He (何伟), Maolin Liu (刘懋霖), Xiangjun Peng (彭祥军),  Fengxian Xin (辛锋先), and Tian Jian Lu (卢天健)



View Online



Export Citation



CrossMark

Physics of Fluids

SPECIAL TOPIC: Tribute to
Frank M. White on his 88th Anniversary

SUBMIT TODAY!



Sound absorption of petal shaped micro-channel porous materials

Cite as: Phys. Fluids **33**, 063606 (2021); doi: [10.1063/5.0053059](https://doi.org/10.1063/5.0053059)

Submitted: 4 April 2021 · Accepted: 30 May 2021 ·

Published Online: 15 June 2021




View Online



Export Citation



CrossMark

Wei He (何伟),^{1,2} Maolin Liu (刘懋霖),^{1,2} Xiangjun Peng (彭祥军),^{1,2} Fengxian Xin (辛锋先),^{1,2,a)}  and Tian Jian Lu (卢天健)^{3,4,b)}

AFFILIATIONS

¹State Key Laboratory for Strength and Vibration of Mechanical Structures, Xi'an Jiaotong University, Xi'an 710049, People's Republic of China

²MOE Key Laboratory for Multifunctional Materials and Structures, Xi'an Jiaotong University, Xi'an 710049, People's Republic of China

³State Key Laboratory of Mechanics and Control of Mechanical Structures, Nanjing University of Aeronautics and Astronautics, Nanjing 210016, People's Republic of China

⁴MIIT Key Laboratory of Multi-functional Lightweight Materials and Structures, Nanjing University of Aeronautics and Astronautics, Nanjing 210016, People's Republic of China

^{a)}Author to whom correspondence should be addressed: fengxian.xin@gmail.com

^{b)}Electronic mail: tjlu@nuaa.edu.cn

ABSTRACT

Experiments demonstrated that surface roughness could significantly improve the sound absorption performance of porous materials. In this study, to quantitatively explore the underlying physical mechanisms, porous materials with roughened pore surfaces are modeled as a bundle of parallel petal shaped tubes, so that relevant acoustic transport parameters, namely, viscous permeability, thermal permeability, tortuosity, viscous characteristic length, and thermal characteristic length, can be theoretically predicted. Multi-scale numerical simulations are implemented to validate the theoretical predictions, with good agreement achieved. Compared with smooth tubes, petal shaped tubes reduce the viscous and thermal characteristic lengths as well as the viscous and thermal permeabilities, resulting in enhanced sound absorption over a wide frequency band.

Published under an exclusive license by AIP Publishing. <https://doi.org/10.1063/5.0053059>

I. INTRODUCTION

Porous materials, such as packed spheres,^{1,2} foams,^{3–5} and fibrous sheets,^{6,7} are widely used to absorb noise, as friction and thermal exchange between air and solid frame dissipate part of acoustic energy into useless heat, thus reducing noise intensity. During the propagation of sound wave, the frame of a porous material may be considered rigid, for the bulk modulus of solid is usually much greater than that of air. Equivalently, the porous material may be replaced by a layer of imaginary fluid. To this end, under the assumption of linearity, by decoupling the viscous and thermal effects of air, the frequency-dependent effective density and bulk modulus of the porous material can be derived.^{8–10}

The solid walls of a porous material are typically of sub-millimeter scale and are, strictly speaking, uneven (i.e., roughened), mainly due to processing difficulties at such small scale. In fluid mechanics, it is known that the presence of surface roughness could

severely disturb fluid flow.^{11–19} However, thus far, there is not much work devoted to studying, either experimentally or theoretically, the effect of surface roughness on sound propagation in porous materials. Experimentally, it was reported that the static flow resistance of open-celled aluminum foam was enlarged by about 72% after micro-rods were randomly synthesized on the surfaces of individual pores, and these significantly roughened pore surfaces led to sound absorption enhanced over a wide frequency range;²⁰ similarly, sintered fibrous sheets made of roughened copper fibers also exhibited improved sound absorption.²¹ Theoretically, Meng *et al.*²² studied sound propagation in a rough micro-tube with surface-mounted cylinders, finding that surface roughness elevated acoustic resistance and enlarged sound absorption coefficient. Xu *et al.*²³ modeled porous materials as a bundle of tubes having sinusoidal surface roughness (i.e., longitudinal surface roughness) along the incident direction of sound waves. It was demonstrated that surface roughness weakened thermal dissipation

but strengthened viscous dissipation, thus shifting the sound absorption peak toward a lower frequency.

This study aims to quantify the influence of circumferential surface roughness (i.e., transverse roughness that is perpendicular to the incident direction of sound) on sound absorption by idealizing the porous material as a bundle of parallel petal shaped tubes. Acoustic transport parameters of the Johnson–Champoux–Allard–Lafarge (JCAL) model are then theoretically derived to determine the surface impedance and sound absorption coefficient of the idealized porous material. To verify the theoretical predictions and reveal the mechanism underlying the influence of surface roughness on sound absorption, multi-scale numerical simulations are implemented with the commercial finite element code COMSOL Multiphysics. Although the roughened pore morphology is ideally considered as petal shaped, other morphologies, like equilateral triangular and regular quadrilateral, can also be analyzed by decomposing the pore shape function into a series of trigonometric functions with the help of the Fourier transform method.²⁴

II. THEORETICAL MODEL

As shown in Fig. 1(a), the porous material with interior roughened surfaces intended for sound absorption is made of a series of periodically placed, parallel petal shaped tubes. Here, the petal shape is considered as the circumferential roughness of the inside surface of the tubes. The sound absorber is backed by a rigid wall, and the sound wave is incident vertically on the front surface. Due to periodicity, a unit cell [Fig. 1(b)] is extracted to simplify subsequent analysis. The length and width of the unit cell are both l , and the thickness is h . Figure 1(c) presents the cross section of the petal shaped tube, which has a mean diameter of D and a roughness amplitude of e . In polar coordinates, the tube radius $r(\theta)$ at polar angle θ is given by

$$r(\theta) = D[0.5 - \varepsilon \sin(n\theta)], \tag{1}$$

where $\varepsilon = e/D$ is the relative roughness, and n is a positive integer representing the number of rough elements in tube section.

Under the excitation of harmonic sound wave, the air velocity \mathbf{v} and the excess temperature τ in a porous material with open cells are related to the sound pressure p as^{8,10}

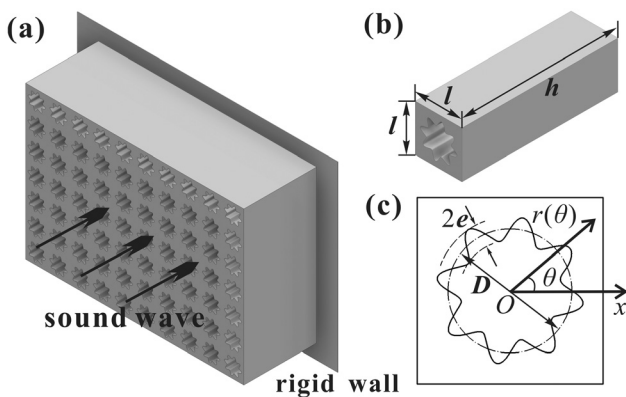


FIG. 1. Schematic of porous material composed of periodic parallel petal shaped tubes: (a) overall three-dimensional diagram; (b) unit cell; and (c) cross section of unit cell.

$$\phi \langle \mathbf{v} \rangle = -\frac{k(\omega)}{\mu} \nabla \langle p \rangle, \tag{2}$$

$$\phi \langle \tau \rangle = \frac{k'(\omega)}{\kappa} \frac{\partial \langle p \rangle}{\partial t}, \tag{3}$$

where ϕ is the porosity, ω is the angular frequency of incident sound wave, $k(\omega)$ is the dynamic viscous permeability, $k'(\omega)$ is the dynamic thermal permeability, μ and κ are the viscosity coefficient and the thermal conductivity of air, respectively, and $\langle \rangle$ denotes a volume average operator over the representative elementary volume.

When the frequency of sound tends to 0 Hz, the dynamic viscous permeability and thermal permeability approach their corresponding static values, as

$$\lim_{\omega \rightarrow 0} k(\omega) = k_0, \tag{4}$$

$$\lim_{\omega \rightarrow 0} k'(\omega) = k'_0, \tag{5}$$

where k_0 is the static viscous permeability and k'_0 is the static thermal permeability. In this case, Eq. (2) is simplified as $\phi \langle \mathbf{v} \rangle = -k_0 \nabla \langle p \rangle / \mu$, which is exactly the Darcy's law.

In the high frequency limit (i.e., $\omega \rightarrow \infty$), the asymptotic expressions of $k(\omega)$ and $k'(\omega)$ are given as^{8–10}

$$k(\omega) = \frac{\mu \phi}{-j \omega \alpha_\infty} \left[1 - (1+j) \frac{\delta}{\Lambda} \right], \tag{6}$$

$$k'(\omega) = \frac{\mu' \phi}{-j \omega} \left[1 - (1+j) \frac{\delta'}{\Lambda'} \right], \tag{7}$$

where $\mu' = \kappa / (\rho_0 c_p)$, ρ_0 is the air density, c_p is the specific heat capacity at constant pressure, α_∞ is the tortuosity, $\delta = \sqrt{2\mu / (\rho_0 \omega)}$ is the viscous skin depth, $\delta' = \sqrt{2\mu' / \omega}$ is the thermal skin depth, Λ and Λ' denote the viscous and thermal characteristic length, respectively, and $j = \sqrt{-1}$ is the imaginary unit.

According to the previous results for two extreme cases, the dynamic viscous permeability and thermal permeability in the intermediate frequency range can be approximated as¹⁰

$$k(\omega) = \frac{k_0}{\sqrt{1 - j \frac{M \omega k_0 \alpha_\infty}{2\mu \phi} - j \frac{\omega k_0 \alpha_\infty}{\mu \phi}}}, \tag{8}$$

$$k'(\omega) = \frac{k'_0}{\sqrt{1 - j \frac{M' \omega k'_0}{2\mu' \phi} - j \frac{\omega k'_0}{\mu' \phi}}}, \tag{9}$$

where $M = (8\alpha_\infty k_0) / (\phi \Lambda^2)$ is the dimensionless viscous shape factor, and $M' = (8k'_0) / (\phi \Lambda'^2)$ is the dimensionless thermal shape factor.

At the macroscopic level, the propagation of sound in a porous material is governed by

$$\rho_0 \alpha(\omega) \frac{\partial \langle \mathbf{v} \rangle}{\partial t} = -\nabla \langle p \rangle, \tag{10}$$

$$\frac{\beta(\omega)}{K} \frac{\partial \langle p \rangle}{\partial t} = -\nabla \cdot \langle \mathbf{v} \rangle, \tag{11}$$

where $\alpha(\omega)$ is the dynamic tortuosity, $\beta(\omega)$ is the scaled dynamic compressibility, $K = \gamma P_0$ is the bulk modulus of air, γ is the specific

heat ratio of air, and P_0 is the ambient pressure. From Eqs. (2) and (10), the dynamic tortuosity is related to the dynamic viscous permeability as

$$\alpha(\omega) = -\frac{\mu\phi}{j\omega k(\omega)}, \tag{12}$$

while the scaled dynamic compressibility is related to the dynamic thermal permeability as¹⁰

$$\beta(\omega) = \gamma + (\gamma - 1) \frac{j\omega}{\mu' \phi} k'(\omega). \tag{13}$$

Based on Eqs. (10) and (11), the effective density $\rho_{eq}(\omega)$ and effective bulk modulus $K_{eq}(\omega)$ of a porous material can be defined as

$$\rho_{eq}(\omega) = \rho_0 \alpha(\omega) = \rho_0 \alpha_\infty \left[1 + \frac{\mu\phi}{j\omega\rho_0 k_0 \alpha_\infty} \sqrt{1 + j \frac{4\alpha_\infty^2 k_0^2 \omega \rho_0}{\mu\phi^2 \Lambda^2}} \right], \tag{14}$$

$$K_{eq}(\omega) = K/\beta(\omega) = \gamma P_0 / \left\{ \gamma - (\gamma - 1) / \left[1 - j \frac{\phi\kappa}{k_0' C_p \rho_0 \omega} \sqrt{1 + j \frac{4k_0'^2 c_p \rho_0 \omega}{\kappa \Lambda'^2 \phi^2}} \right] \right\}. \tag{15}$$

Equations (14) and (15) constitute the well-known semi-phenomenological JCAL model, requiring five parameters, namely, viscous permeability k_0 , thermal permeability k_0' , tortuosity α_∞ , viscous characteristic length Λ , and thermal characteristic length Λ' . These are transport parameters of the porous material, each determined by its pore morphology.

The viscous permeability is inversely proportional to the static flow resistance σ_m of the porous material as follows:

$$k_0 = \frac{\mu}{\sigma_m}. \tag{16}$$

Given that the porous material studied here is composed of parallel tubes, σ_m can be characterized by the static flow resistance of a single tube σ_t as $\sigma_m = \sigma_t/\phi$. For incompressible viscous fluid flow in a petal shaped tube, σ_t has been theoretically obtained at low Reynolds numbers using the perturbation method as follows.²⁴

$$\sigma_t = \frac{32\mu}{D^2} \left\{ \frac{1}{(1 - 2\varepsilon)^4} + \left(1 - \frac{1}{(1 - 2\varepsilon)^4} \right) \frac{2e^{-\frac{1}{12.5n}}}{1 + e^{-\frac{1}{12.5n}}} \right\}. \tag{17}$$

If the tube is circular with diameter D , the flow resistance is $\sigma_t = 32\mu/D^2$.

The tortuosity α_∞ , the viscous characteristic length Λ , and the thermal characteristic length Λ' are all defined in the high frequency limit, where the porous material is thought to be filled with an ideal inviscid fluid, as

$$\alpha_\infty = \langle \mathbf{v}^2(\mathbf{r}_i) \rangle / \langle \mathbf{v}(\mathbf{r}_i) \rangle^2, \tag{18}$$

$$\frac{2}{\Lambda} = \frac{\int_A \mathbf{v}^2(\mathbf{r}_w) dA}{\int_V \mathbf{v}^2(\mathbf{r}_i) dV}, \tag{19}$$

$$\frac{2}{\Lambda'} = \frac{\int_A dA}{\int_V dV}, \tag{20}$$

where $\mathbf{v}(\mathbf{r}_i)$ is the local velocity of inviscid fluid inside the pore, $\mathbf{v}(\mathbf{r}_w)$ is the velocity of inviscid fluid on the solid–fluid interface, and A and V denote the surface area and volume of the pore, respectively.

For inviscid flow in a straight-through petal shaped tube, the velocity at any point is equal. Thus, the velocity-related terms in the numerator and denominator of Eqs. (18) and (19) can be removed, resulting in

$$\alpha_\infty = 1, \tag{21}$$

$$\Lambda = \Lambda' = 2 \frac{\int_V dV}{\int_A dA} = \frac{D \int_0^{2\pi} [0.5 - \varepsilon \sin(n\theta)]^2 d\theta}{\int_0^{2\pi} \sqrt{[0.5 - \varepsilon \sin(n\theta)]^2 + [-\varepsilon n \cos(n\theta)]^2} d\theta}. \tag{22}$$

The thermal permeability k_0' describes thermal exchange between the solid frame and the fluid in the low frequency limit. As it is difficult to deduce an analytical expression of the dimensionless thermal shape factor according to pore morphology, an approximate expression $k_0' = \phi\Lambda'^2/8$ proposed by Champoux and Allard⁹ is adopted.

Once the transport parameters of the porous material are determined, its effective density and effective bulk modulus are also determined, so that its characteristic impedance Z and the wavenumber k can be calculated as

$$Z = \sqrt{\rho_{eq}(\omega) K_{eq}(\omega)}, \tag{23}$$

$$k = \omega \sqrt{\frac{\rho_{eq}(\omega)}{K_{eq}(\omega)}}. \tag{24}$$

If the porous material is backed by a rigid wall, the relative surface impedance is given by

$$z_s = -jZ \cot(kh) / (\phi Z_0), \tag{25}$$

where $Z_0 = \rho_0 c_0$ is the characteristic impedance of air and c_0 is the sound speed in air.

Finally, the sound absorption coefficient of the porous sound absorber having roughened pores is defined as the ratio of acoustic energy absorbed to incident acoustic energy, given by

$$\alpha = \frac{4\text{Re}(z_s)}{[\text{Re}(z_s) + 1]^2 + \text{Im}(z_s)^2}, \tag{26}$$

where $\text{Re}()$ and $\text{Im}()$ denote the real and imaginary part of a complex, respectively.

III. THE MULTI-SCALE NUMERICAL SIMULATION METHOD

As the frequency of sound approaches 0 Hz, the influence of viscosity on fluid flow is far more than that of inertia. In this case, fluid motion is governed by the static Stokes equation, with no-slip boundary applied at solid–fluid interface. By introducing the scaled velocity

\mathbf{k}_0 and the associated scalar pressure q_0 , the governing equation and boundary condition can be rewritten as^{25,26}

$$\Delta \mathbf{k}_0 = \nabla q_0 - \mathbf{e} \quad \text{in } \Omega_f, \tag{27}$$

$$\nabla \cdot \mathbf{k}_0 = 0 \quad \text{in } \Omega_f, \tag{28}$$

$$\mathbf{k}_0 = \mathbf{0} \quad \text{on } \partial\Omega_{sf}, \tag{29}$$

where the unit vector \mathbf{e} represents a pressure gradient along the incident direction of sound wave, Ω_f is the fluid domain, and $\partial\Omega_{sf}$ represents the solid–fluid interface. The viscous permeability of the porous material k_0 is defined as

$$k_0 = \phi \langle k_0^m \rangle, \tag{30}$$

where k_0^m is the scaled velocity along the incident direction of sound wave.

In the limit $\omega \rightarrow \infty$, the viscous skin depth tends to zero. Therefore, the fluid can be considered as a perfect one without viscosity, and its motion is mainly controlled by inertia. The flow of a perfect fluid in the porous material is similar to the flow of a conductive fluid within insulating solid skeletons as follows:^{27,28}

$$\mathbf{E} = \mathbf{e}' - \nabla q \quad \text{in } \Omega_f, \tag{31}$$

$$\nabla \cdot \mathbf{E} = 0 \quad \text{in } \Omega_f, \tag{32}$$

where \mathbf{E} is the local electric field, the unit vector \mathbf{e}' denotes the externally applied electric field, and q is the disturbed electric potential. At the solid–fluid interface, the boundary condition of insulation is satisfied as follows:

$$\mathbf{E} \cdot \mathbf{n} = 0 \quad \text{on } \partial\Omega_{sf}, \tag{33}$$

where \mathbf{n} is the outward normal. The tortuosity α_∞ , the viscous characteristic length Λ , and the thermal characteristic length Λ' are determined as

$$\alpha_\infty = \frac{\langle \mathbf{E} \cdot \mathbf{E} \rangle}{\langle \mathbf{E} \rangle \cdot \langle \mathbf{E} \rangle}, \tag{34}$$

$$\Lambda = 2 \frac{\int_{\Omega_f} \mathbf{E} \cdot \mathbf{E} dV}{\int_{\partial\Omega_{sf}} \mathbf{E} \cdot \mathbf{E} dS}, \tag{35}$$

$$\Lambda' = 2 \frac{\int_{\Omega_f} dV}{\int_{\partial\Omega_{sf}} dS}. \tag{36}$$

During the propagation of sound wave, the sound pressure is oscillatory; thus the air cyclically undergoes compression and expansion, and the temperature changes accordingly. Lafarge *et al.*¹⁰ introduced the thermal permeability k' to link the excess temperature τ with the harmonic sound pressure p as: $\tau = i\omega p k' / \kappa$. In the low frequency limit (i.e., $\omega \rightarrow 0$), the static thermal permeability k'_0 satisfies the Poisson equation and the Dirichlet boundary condition as follows:²⁵

$$-\Delta k'_0 = 1 \quad \text{in } \Omega_f, \tag{37}$$

$$k'_0 = 0 \quad \text{on } \partial\Omega_{sf}. \tag{38}$$

The static thermal permeability k'_0 is then calculated as

$$k'_0 = \phi \langle k'_0 \rangle. \tag{39}$$

The above three sets of partial differential equations (PDEs) are solved in the Creep Flow module, the Electrostatics module, and the Coefficient Form PDE module of COMSOL Multiphysics, respectively. With the viscosity and density of fluid in the Creep Flow module set as $1 \text{ Pa} \cdot \text{s}$ and 1 kg/m^3 , the governing equation of fluid flow is the same as Eq. (27). The pressure gradient \mathbf{e} and the electric field \mathbf{e}' are externally applied by separately presetting the pressure and electric potential of the inlet and outlet. Upon substituting the numerically calculated transport parameters into the JCAL model, the effective impedance and sound absorption coefficient are obtained.

IV. RESULTS AND DISCUSSION

In the following analysis, the relevant geometric parameters are adopted as: $D = 0.6 \text{ mm}$, $\varepsilon = 0.1$, $n = 8$, $h = 30 \text{ mm}$, $l = 0.9 \text{ mm}$, $\phi = 34.91\%$. The optimal cell size of the sound-absorbing porous material is on the order of 0.1 mm , which varies slightly with the frequency.²⁹ If the pore size is too small, the large acoustic resistance of the porous material will prevent sound waves from entering. On the other hand, the acoustic energy is mainly dissipated in the boundary layer of the pore wall. If the pore size is too large, the energy dissipation near the center of the pore is negligible, and the sound absorption potential of the porous material cannot be fully utilized. Therefore, medium-sized tubes with a diameter of $D = 0.6 \text{ mm}$ are chosen to form the porous material. In the theoretical model, to ensure the prediction accuracy of the flow resistance of petal shaped tubes, the relative roughness ε should not exceed 0.1^{24} . The number of rough elements n in the tube section is not limited. As the thickness of the porous material increases, the air propagation path is extended, which significantly improves the low-frequency sound absorption performance of the porous material. However, if the porous material is too thick, it will occupy more space. In order to improve the sound absorption performance and reduce the occupied space as much as possible, the thickness of the porous material h is set to 30 mm . The porosity ϕ of porous materials is related to the distance l between tubes. To avoid overlapping of the tubes, the distance between the tubes should be greater than $D(1 + 2\varepsilon)$. If the tube spacing is too large, the interior surface of porous material will be reduced, and the sound absorption effect will decrease. Therefore, $l = 0.9 \text{ mm}$ is also a compromise choice. The related thermal physical parameters of air are given in Table I.

TABLE I Thermo-physical parameters of air at 298.15 K.

Thermo-physical parameter	Symbol	Unit	Value
Density	ρ_0	kg m^{-3}	1.18
Sound speed	c_0	m/s	346.30
Viscosity coefficient	η	$\text{Pa} \cdot \text{s}$	1.85×10^{-5}
Specific heat ratio	γ	1	1.4018
Ambient pressure	P_0	kPa	101.33
Specific heat capacity	c_p	$\text{J}/(\text{kg K})$	1006.6
Thermal conductivity	κ	$\text{W}/(\text{m K})$	0.025

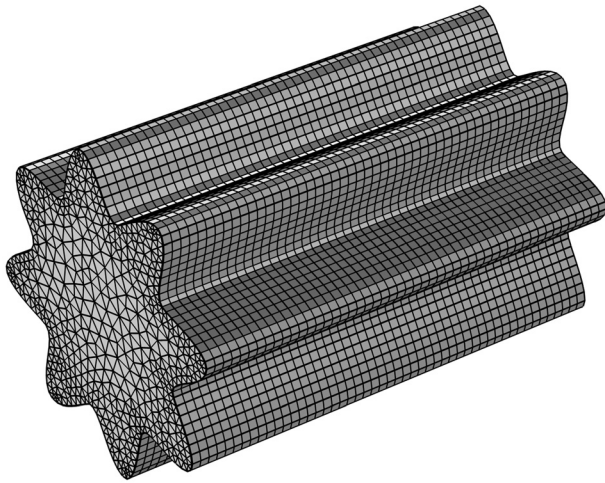


FIG. 2. Finite element mesh of computational domain.

For the cross section of the tube does not change along its axial direction, as presented in Fig. 2, only the air domain in a segment (length: 1 mm) of petal shaped tube is modeled to numerically calculate the related transport parameters.

Table II lists the theoretically predicted and numerically calculated transport parameters using the model of Figs. 1 and 2. Except for the case of thermal permeability, the theoretical predictions are in good agreement with the simulation results. This is because the theoretical model does not specifically consider the influence of pore morphology on thermal permeability; instead, an approximate expression $k'_0 = \phi \Lambda^2 / 8$ is used to estimate this parameter. However, subsequent analysis results show that the effect of thermal permeability on sound absorption is far less than that of viscous permeability. Therefore, the current theoretical model is accurate enough to predict the sound absorption performance of a porous material with roughened pore surfaces.

Substituting the transport parameters listed in Table II into the JCAL model enables determining the effective density and bulk modulus of the equivalent fluid, and then calculating the sound absorption coefficient. As shown in Fig. 3, the sound absorption coefficient predicted by the theoretical model is consistent with the numerical simulation results, thus proving the negligible effect of thermal permeability. For further comparison, the same process is implemented for porous materials with smooth pore surfaces ($\varepsilon = 0$). At all

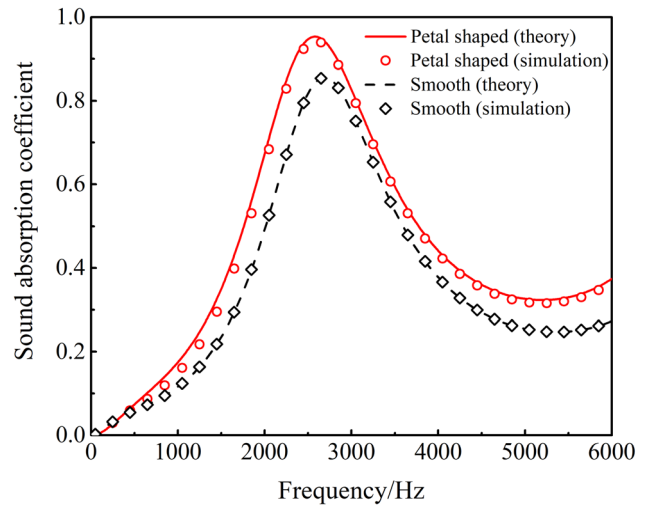


FIG. 3. Sound absorption coefficient plotted as a function of frequency: comparison between petal shaped and smooth tubes.

frequencies, the sound absorption performance of the porous material with roughened surfaces is better than that with smooth surfaces.

When a sound wave is incident upon a porous material, part of the acoustic energy is absorbed and the rest is reflected. To absorb sound as much as possible, Eq. (26) shows that the real and imaginary parts of the relative surface impedance must be close to 1 and 0, respectively. Figure 4 compares the relative acoustic surface impedance of the porous material having roughened pore surfaces with that having smooth ones. As can be seen, in the presence of roughened surfaces, the sound absorption coefficient reaches the peak of 0.9532 at 2580 Hz; correspondingly, the real part of relative acoustic surface impedance is 0.6480, while the imaginary part is 0.0586. In the case of smooth surfaces, the sound absorption achieves the maximum value of 0.8556 at 2680 Hz, with the real part of relative acoustic surface impedance equal to 0.4519 and the imaginary part equal to 0.0680.

In Fig. 5, the numerically calculated distributions of viscous permeability and thermal permeability on the cross section of a petal shaped tube are compared to those of a smooth tube. In the region near the tube wall, the flow of air is severely impeded so that the velocity is smaller relative to other areas, thus yielding a smaller viscous permeability. For porous materials, the solid–fluid interfaces of porous materials are all considered as isothermal boundaries. The thermal conductivity of solid is in general larger than that of air; thus, heat can be conducted quickly across the solid skeleton when sound waves

TABLE II. Theoretical predictions and numerical results of transport parameters.

Acoustic parameter	Symbol	unit	Theoretical prediction	Numerical simulation
Viscous permeability	k_0	mm ²	2.7698×10^{-3}	2.8055×10^{-3}
Thermal permeability	k'_0	mm ²	1.9029×10^{-3}	2.7133×10^{-3}
Tortuosity	α_∞	1	1	1
Viscous characteristic length	Λ	mm	0.20677	0.20977
Thermal characteristic length	Λ'	mm	0.20677	0.20977

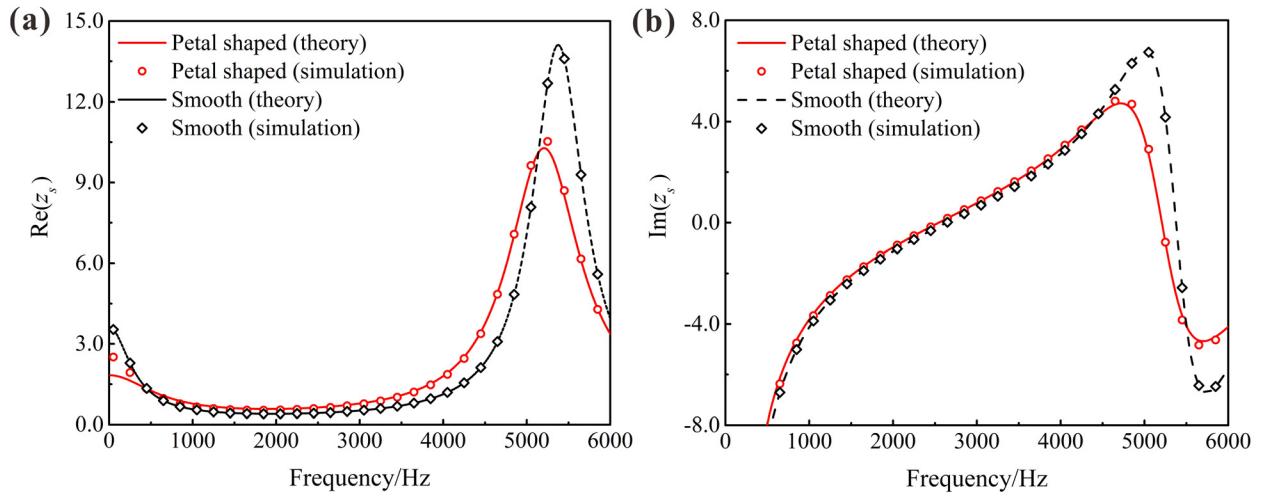


FIG. 4. (a) Real part and (b) imaginary part of relative acoustic surface impedance: comparison between petal shaped and smooth tubes.

propagate in the porous material. Since the density and specific heat capacity of solid are also much larger than that of gas, the temperature change of solid–fluid interfaces is negligible and approximately set to zero. Therefore, temperature change of the air near the solid wall is smaller in comparison with other areas, which leads to a smaller thermal permeability.

The influence of surface roughness on transport parameters is displayed in Fig. 6. Since the petal shaped tube is straight, the tortuosity remains 1 in all cases. The results of Fig. 6 reveal that, as the relative roughness or number of rough elements increases, the viscous/thermal characteristic length and the viscous/thermal permeability of porous materials all decrease. This is because, when the relative roughness or number of rough elements increases, the contact area between the air

and the interior wall of the porous material is enlarged, thus intensifying friction and thermal exchange between the air and solid skeleton.

Figure 7 presents the predicted influence of surface roughness on sound absorption. With the number of rough elements fixed at 8, as the relative roughness increases, the frequency at the absorption peak does not change much, but the absorption bandwidth is widened. In contrast, with the relative roughness fixed at 0.1, as the number of rough elements is increased, the absorption peak is shifted to a lower frequency and the absorption performance is increasingly enhanced. More specifically, for the porous material with smooth surfaces ($n = 0$), the first sound absorption peak of 0.8556 appears at 2680 Hz, and the average sound absorption coefficient in the whole frequency range is 0.3621, while, for the porous material with roughened surfaces ($n = 16$), the first sound absorption peak moves to 2340 Hz with the peak value increased by 16.85% to 0.9998. The average sound absorption coefficient reaches 0.5290, an increase of 46.09%.

V. CONCLUSIONS

A combined theoretical modeling and numerical simulation approach is developed to investigate the influence of the surface roughness on sound absorption of porous material idealized as a bundle of parallel petal shaped micro-channel tubes. The petal shape is considered as the circumferential roughness of the inside surface of the tubes. Based on the proposed pore morphology, key acoustic transport parameters pertinent to the Johnson–Champoux–Allard–Lafarge (JCAL) model are theoretically obtained, which are then verified via multi-scale numerical simulations. Results show that the circumferential roughened surfaces (i.e., the petal shaped) increase the contact area between the air and solid skeleton of porous materials, resulting in increased friction and heat exchange losses. Compared with porous materials with smooth surfaces, the roughened pore surfaces improve the sound absorption performance in a wide frequency range. By changing the roughness of pore surfaces, the acoustic performance of porous materials can be effectively adjusted, which provides guidance for the sound absorption design of porous materials.

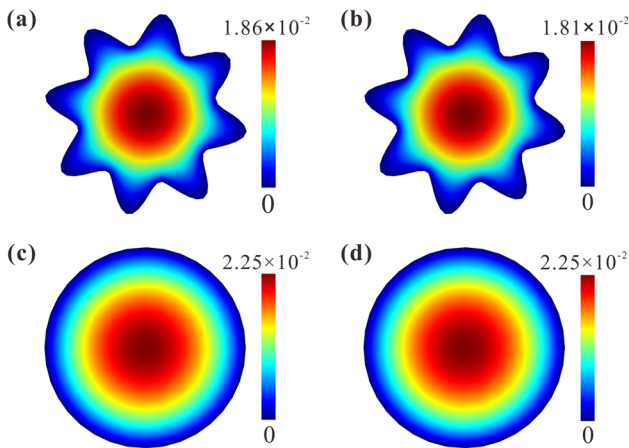


FIG. 5. Numerical results of permeability fields: (a) viscous permeability of petal shaped tube (mm^2); (b) thermal permeability of petal shaped tube (mm^2); (c) viscous permeability of smooth tube (mm^2); and (d) thermal permeability of smooth tube (mm^2).

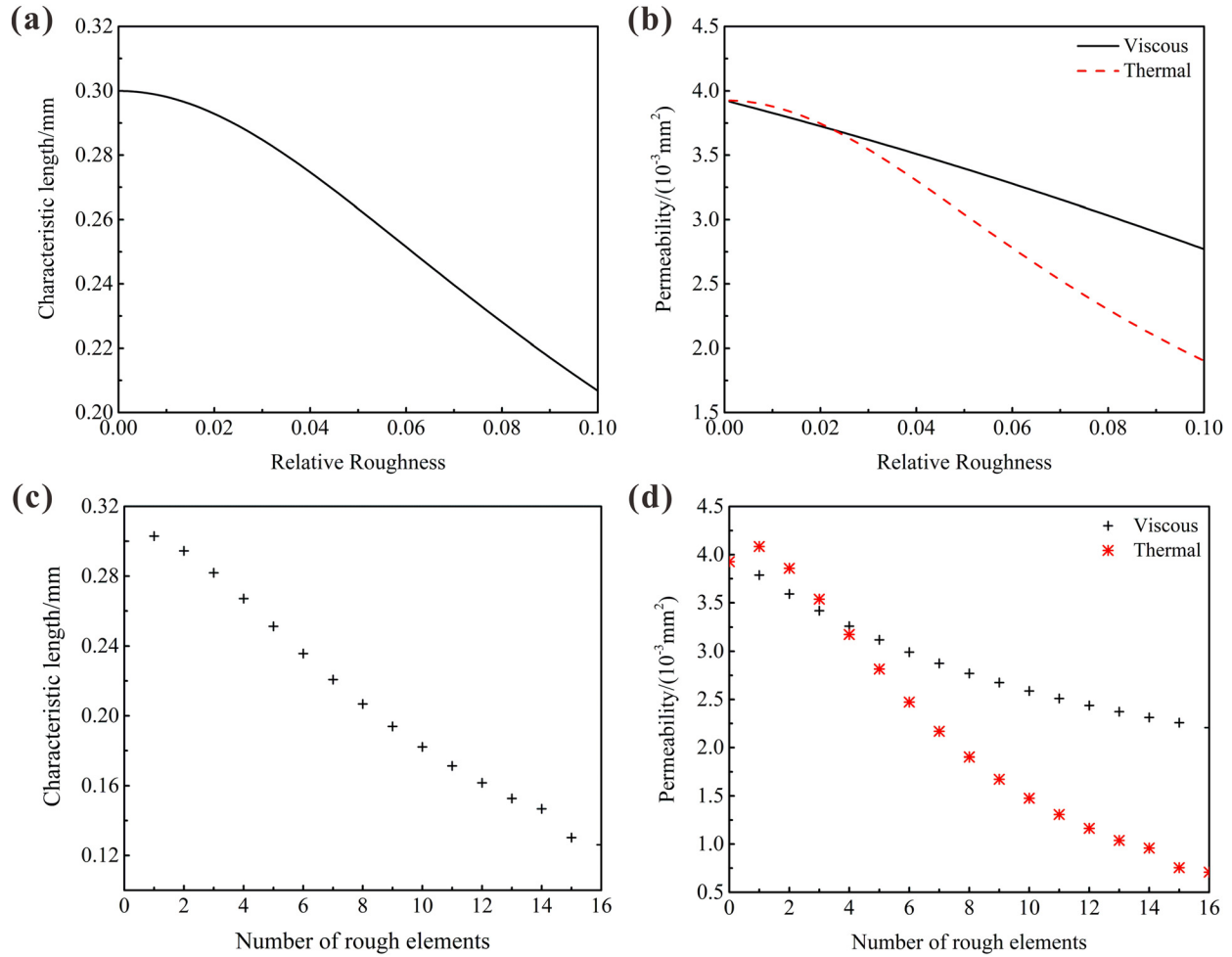


FIG. 6. Influence of relative roughness on (a) characteristic length ($n=8$) and (b) permeability ($n=8$). Influence of the number of rough elements on (c) characteristic length ($\varepsilon=0.1$) and (d) permeability ($\varepsilon=0.1$).

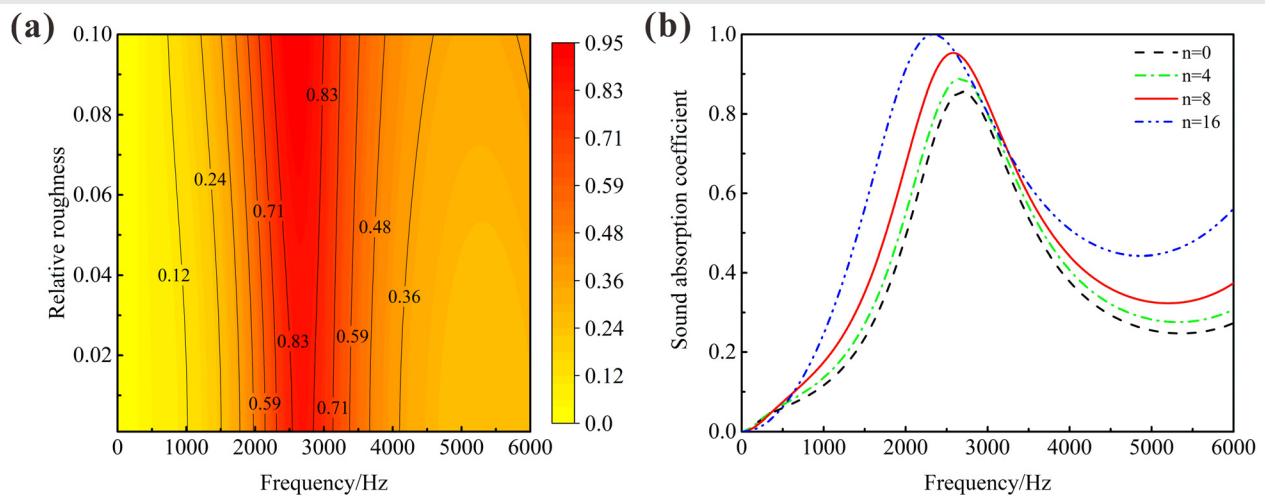


FIG. 7. (a) Influence of relative roughness on sound absorption coefficient ($n=8$) and (b) influence of the number of rough elements on sound absorption coefficient ($\varepsilon=0.1$).

ACKNOWLEDGEMENTS

This work was supported by the National Natural Science Foundation of China (Nos. 52075416, 11772248, 11972185, and 12032010).

DATA AVAILABILITY

The data that support the findings of this study are available from the corresponding author upon reasonable request.

REFERENCES

- ¹S. Gasser, F. Paun, and Y. Brechet, "Absorptive properties of rigid porous media: Application to face centered cubic sphere packing," *J. Acoust. Soc. Am.* **117**, 2090–2099 (2005).
- ²C. Y. Lee, M. J. Leamy, and J. H. Nadler, "Acoustic absorption calculation in irreducible porous media: A unified computational approach," *J. Acoust. Soc. Am.* **126**, 1862–1870 (2009).
- ³T. J. Lu, A. Hess, and M. F. Ashby, "Sound absorption in metallic foams," *J. Appl. Phys.* **85**, 7528–7539 (1999).
- ⁴O. Doutres, N. Atalla, and K. Dong, "A semi-phenomenological model to predict the acoustic behavior of fully and partially reticulated polyurethane foams," *J. Appl. Phys.* **113**, 054901 (2013).
- ⁵C. Teruna, F. Manegar, F. Avallone, D. Ragni, D. Casalino, and T. Carolus, "Noise reduction mechanisms of an open-cell metal-foam trailing edge," *J. Fluid Mech.* **898**, A18 (2020).
- ⁶S. Ren, Q. Ao, H. Meng, F. Xin, L. Huang, C. Zhang, and T. J. Lu, "A semi-analytical model for sound propagation in sintered fiber metals," *Composites, Part B* **126**, 17–26 (2017).
- ⁷P. Soltani and M. Norouzi, "Prediction of the sound absorption behavior of nonwoven fabrics: Computational study and experimental validation," *J. Sound Vib.* **485**, 115607 (2020).
- ⁸D. L. Johnson, J. Koplik, and R. Dashen, "Theory of dynamic permeability and tortuosity in fluid-saturated porous media," *J. Fluid Mech.* **176**, 379–402 (1987).
- ⁹Y. Champoux and J. F. Allard, "Dynamic tortuosity and bulk modulus in air-saturated porous media," *J. Appl. Phys.* **70**, 1975–1979 (1991).
- ¹⁰D. Lafarge, P. Lemarinier, J. F. Allard, and V. Tarnow, "Dynamic compressibility of air in porous structures at audible frequencies," *J. Acoust. Soc. Am.* **102**, 1995–2006 (1997).
- ¹¹S. Song, X. Yang, F. Xin, and T. J. Lu, "Modeling of surface roughness effects on Stokes flow in circular pipes," *Phys. Fluids* **30**, 023604 (2018).
- ¹²Y. Lu, H. Liu, Z. Liu, and C. Yan, "Investigation and parameterization of transition shielding in roughness-disturbed boundary layer with direct numerical simulations," *Phys. Fluids* **32**, 074110 (2020).
- ¹³S. Goswami and A. Hemmati, "Response of turbulent pipeflow to multiple square bar roughness elements at high Reynolds number," *Phys. Fluids* **32**, 075110 (2020).
- ¹⁴Y. Kuwata and R. Nagura, "Direct numerical simulation on the effects of surface slope and skewness on rough-wall turbulence," *Phys. Fluids* **32**, 105113 (2020).
- ¹⁵I. Arenas, E. García, M. K. Fu, P. Orlandi, M. Hultmark, and S. Leonardi, "Comparison between super-hydrophobic, liquid infused and rough surfaces: A direct numerical simulation study," *J. Fluid Mech.* **869**, 500–525 (2019).
- ¹⁶N. N. Anika, L. Djenidi, and S. Tardu, "Roughness effect in an initially laminar channel flow," *J. Fluid Mech.* **892**, A34 (2020).
- ¹⁷X. Fang, Z. Yang, B.-C. Wang, M. F. Tachie, and D. J. Bergstrom, "Large-eddy simulation of turbulent flow and structures in a square duct roughened with perpendicular and V-shaped ribs," *Phys. Fluids* **29**, 065110 (2017).
- ¹⁸J. Javaherchian and A. Moosavi, "Pressure drop reduction of power-law fluids in hydrophobic microgrooved channels," *Phys. Fluids* **31**, 073106 (2019).
- ¹⁹S. Raayai-Ardakani and G. H. McKinley, "Geometric optimization of riblet-textured surfaces for drag reduction in laminar boundary layer flows," *Phys. Fluids* **31**, 053601 (2019).
- ²⁰Y. Ren, K. Wang, B. Zhu, X. Wang, X. Wang, and F. Han, "Synthesis of ZnO micro-rods on the cell walls of open celled Al foam and their effect on the sound absorption behavior," *Mater. Lett.* **91**, 242–244 (2013).
- ²¹R. Liu, L. Hou, W. Zhou, and Y. Chen, "Design, fabrication and sound absorption performance investigation of porous copper fiber sintered sheets with rough surface," *Appl. Acoust.* **170**, 107525 (2020).
- ²²H. Meng, X. H. Yang, S. W. Ren, F. X. Xin, and T. J. Lu, "Sound propagation in composite micro-tubes with surface-mounted fibrous roughness elements," *Compos. Sci. Technol.* **127**, 158–168 (2016).
- ²³Z. Xu, W. He, F. Xin, and T. J. Lu, "Sound propagation in porous materials containing rough tubes," *Phys. Fluids* **32**, 093604 (2020).
- ²⁴Z. Xu, S. Song, F. Xin, and T. J. Lu, "Mathematical modeling of Stokes flow in petal shaped pipes," *Phys. Fluids* **31**, 013602 (2019).
- ²⁵T. G. Zieliński, "Microstructure-based calculations and experimental results for sound absorbing porous layers of randomly packed rigid spherical beads," *J. Appl. Phys.* **116**, 034905 (2014).
- ²⁶C. Perrot, F. Chevillotte, and R. Panneton, "Dynamic viscous permeability of an open-cell aluminum foam: Computations versus experiments," *J. Appl. Phys.* **103**, 024909 (2008).
- ²⁷M. Avellaneda and S. Torquato, "Rigorous link between fluid permeability, electrical conductivity, and relaxation times for transport in porous media," *Phys. Fluids A* **3**, 2529–2540 (1991).
- ²⁸D. Lafarge, "Comments on 'Rigorous link between fluid permeability, electrical conductivity, and relaxation times for transport in porous media,'" *Phys. Fluids A* **5**, 500–502 (1993).
- ²⁹X. Wang and T. J. Lu, "Optimized acoustic properties of cellular solids," *J. Acoust. Soc. Am.* **106**, 756–765 (1999).